www.czasopisma.pan.pl PAN POLSKA AKADEMIA NAUK www.journals.pan.pl

Arch. Metall. Mater., Vol. 61 (2016), No 2, p. 825–832

DOI: 10.1515/amm-2016-0139

A. GRAJCAR*, B. GRZEGORCZYK*, A. KOZŁOWSKA*,#

CORROSION RESISTANCE AND PITTING BEHAVIOUR OF LOW-CARBON HIGH-Mn STEELS IN CHLORIDE SOLUTION

Corrosion resistance of the X4MnSiAlNbTi27-4-2 and X6MnSiAlNbTi26-3-3 type austenitic steels, after hot deformation as well as after cold rolling, were evaluated in 3.5% NaCl solution using potentiodynamic polarization tests. A type of non-metallic inclusions and their pitting corrosion behaviour were investigated. Additionally, the effect of cold deformation on the corrosion resistance of high-Mn steels was studied. The SEM micrographs revealed that corrosion damage formed in both investigated steels is characterized by various shapes and an irregular distribution at the metallic matrix, independently on the steel state (thermomechanically treated or cold worked). Corrosion pits are generated both in grain interiors, grain boundaries and along the deformation bands. Moreover, corrosion damage is stronger in cold deformed steels in comparison to the thermomechanically treated specimens. EDS analysis revealed that corrosion pits preferentially nucleated on MnS and AlN inclusions or complex oxysulphides. The morphology of corrosion damage in 3.5% NaCl supports the data registered in potentiodynamic tests.

Keywords: high-Mn steel, non-metallic inclusions, SEM, polarization, pitting, effects of strain

1. Introduction

Trends of the modern automotive industry are focused on improvement safety standards and reduction of auto body weight due to the pressure placed on limitation of the amount of harmful gases emitted into the environment. Advanced high strength steels (AHSS) allow to produce lighter automotive bodies leading to reduction of fuel consumption and improvement of the safety of car's users due to their application as energy absorbing elements [1, 2].

The high-manganese alloys belong to 2nd generation of AHSS, which are characterized by high strength and plasticity due to the austenitic microstructure. The combination of mechanical properties depends on many factors, such as chemical composition, heat treatment and metallurgical cleanliness of steel related to the amount of non-metallic inclusions. High-manganese austenitic steels have different types of inclusions, which are formed during melting and casting [3-5]. These steels contain Mn, which combines with sulphur and Si and Al additions with the high chemical affinity to oxygen (Al also to nitrogen). Therefore, the presence of various sulphide and oxide inclusions in these steels can be expected. Park et al. [6] observed inclusions such as MnS, AlN, Al_2O_3, $MnAl_2O_4$ and other complex inclusions in Mn-Al steels. Previous studies [7-9] demonstrated that non-metallic inclusions, especially sulfide inclusions affect the corrosion resistance of steel by providing pitting sites. Presence of MnS inclusions drastically increases corrosion current density and shifts corrosion potential to more negative values. Shibaeva et al. [10] reported that in the passive state, steels with higher sulfur content possess worse passivation and more narrow potential range of the passive state. Experimental observations indicate in many cases that corrosion pits initiate at the inclusion/matrix boundaries. Moreover, the highest electrochemical reactivity of the inclusion/matrix in comparison to the steel matrix and the inclusion itself has been reported [6, 7]. The shape, composition and distribution of inclusions have significant effects on the corrosion resistance, too. Additionally, heat treatment applied and cold deformation have also a significant influence on corrosion behaviour of steel [11]. It is documented [12, 13] that cold deformation drastically increases corrosion current density of steel and consequently increases the amount of corrosion damage. Unfortunately so far, there are no systematic studies on the effects of hot deformation and cold straining on the pitting corrosion resistance of high-Mn steels.

Corrosion properties of stainless steels have been analyzed in many works, however the corrosion resistance of high-Mn steels is not well characterized yet. Therefore, the objective of the present study was to investigate the effect of non-metallic inclusions on the pitting corrosion behaviour of low-carbon X4MnSiAlNbTi27-4-2 and X6MnSiAlNbTi26-3-3 steels in 3.5% NaCl using a potentiodynamic method. Additionally, the effect of cold deformation on corrosion behaviour of the investigated steels has been determined.

2. Experimental details

2.1. Materials and samples

The investigated materials were high-Mn steels with the composition shown in Table 1. Steel ingots were prepared using a vacuum-induction furnace, subsequently hot-forged and roughly rolled to a thickness of 4.5 mm. The next step included

* SILESIAN UNIVERSITY OF TECHNOLOGY, INSTITUTE OF ENGINEERING MATERIALS AND BIOMATERIALS, 18A KONARSKIEGO STR., 44-100 GLIWICE, POLAND

Corresponding author: aleksandra.kozlowska@polsl.pl

thermomechanical processing consisted of austenitizing the samples at 1100°C for 15 minutes, hot rolling of flat samples in 3 passes to a final thickness of about 2 mm at a finishing rolling temperature of 850°C and final water-cooling of the samples to room temperature.

Two groups of specimens were prepared: after thermomechanical rolling (T) and after cold working (CW) – the specimens were cold-strained in a static tensile test to the elongation of 36%.

2.2. Microstructural investigations

Microstructures were examined using optical microscopy – Zeiss Axio Observer Z1m optical microscope. Each sample was ground gradually with 400-1200-grit using SiC paper, polished with Al_2O_3 with granularity of 0.1 μm and then etched using 5% nital to reveal the microstructure.

2.3. Electrochemical measurements

The corrosion properties of the X4MnSiAlNbTi27-4-2 and X6MnSiAlNbTi26-3-3 steels in their different states of treatment (T, CW) were evaluated using the potentiodynamic polarization tests. The corrosion behaviour of the thermomechanically processed (T) specimens was compared to the cold worked (CW) specimens.

A conventional three-electrode configuration was used for the experiment. The working electrodes were made of X4MnSiAlNbTi27-4-2 and X6MnSiAlNbTi26-3-3 steel sheets, with a circular working area of about 0.38 cm^2. A silver/silver chloride (Ag/AgCl) electrode (SSE) was used as a reference electrode, a stainless steel - as a counter electrode. Solution concentration inside the standard silver electrode (SSE) was 3M KCl, with a potential of 0.22 V with respect to hydrogen. Before immersion into the electrolyte, the working area of the specimens was mechanically ground with 1200-grit SiC paper. Then, the samples were polished with Al_2O_3 with granularity of 0.1 μm to create mirror face of each specimen. Prior experiments, all samples were washed in distilled water and rinsed in acetone.

The electrolyte comprised deionised water with sodium chloride. The electrochemical tests were conducted in 3.5% NaCl solution. The pH of the 3.5% sodium chloride solution was about 7. All corrosion tests were conducted using freshly prepared electrolytes. Electrochemical tests were performed at ambient temperatures and all potentials determined in this work refer to SSE.

Electrochemical polarization curves were obtained using an Atlas 0531 Electrochemical Unit potentiostat/galvanostat driven by AtlasCorr05 software. Electrochemical measurements were performed at the scan rate about 1 mV/s. Potentiodynamic scan data were collected to determine the electrochemical parameters: corrosion potential E_{corr} and corrosion current I_{corr} using Tafel slope extrapolation. In order to ensure the reliability of the experimental data, tests were repeated two times for each state of material.

2.4. Pitting morphology observation

Series of potentiodynamic polarization tests in 3.5% NaCl were conducted to investigate the pitting morphology. For scanning electron microscopy (SEM, Zeiss SUPRA 25) all samples after corrosion tests were polished using Al_2O_3 with granularity of 0.1 μm, than cleaned with distilled water and finally etched using 5% nital solution to reveal the austenite grain boundaries and potential initiation sites of pits. To reveal corrosion pits a cover formed on the pit surface has to be removed. The morphology of corrosion damage and composition of non-metallic inclusions were characterized by scanning electron microscope (SEM) using EDS techniques.

3. Results

3.1. Microstructural investigations

Representative microstructures of thermomechanically processed (T) and cold deformed (CW) X6MnSiAlNbTi26-3-3 and X4MnSiAlNbTi27-4-2 steel specimens are shown in Fig. 1a-b and Fig. 2a-b. The microstructures of both thermomechanically treated specimens (Fig. 1a and Fig. 2a) present relatively coarse austenite grains, elongated according to hot rolling direction. Both microstructures contain annealing twins and elongated sulfide inclusions. The mean grain size ware estimated as 80μm. The micrographs in Fig. 1b and Fig. 2b show the X6MnSiAlNbTi26-3-3 and X4MnSiAlNbTi27-4-2 steel specimens after the tensile test performed to the 36% strain. The elongated austenite grains and numerous slip bands can be observed. Additionally, the high amount of deformation twins and presence of elongated sulfide inclusions were identified.

TABLE 1

Chemical composition of the investigated steels (wt. %)

Steel	C	Mn	Si	Al	S	P	Nb	Ti	N	O	Fe
X4MnSiAlNbTi 27-4-2	0.040	27.5	4.18	1.69	0.017	0.004	0.033	0.010	0.0028	0.0006	bal.
X6MnSiAlNbTi 26-3-3	0.065	26.0	3.08	2.87	0.013	0.002	0.034	0.010	0.0028	0.0006	bal.

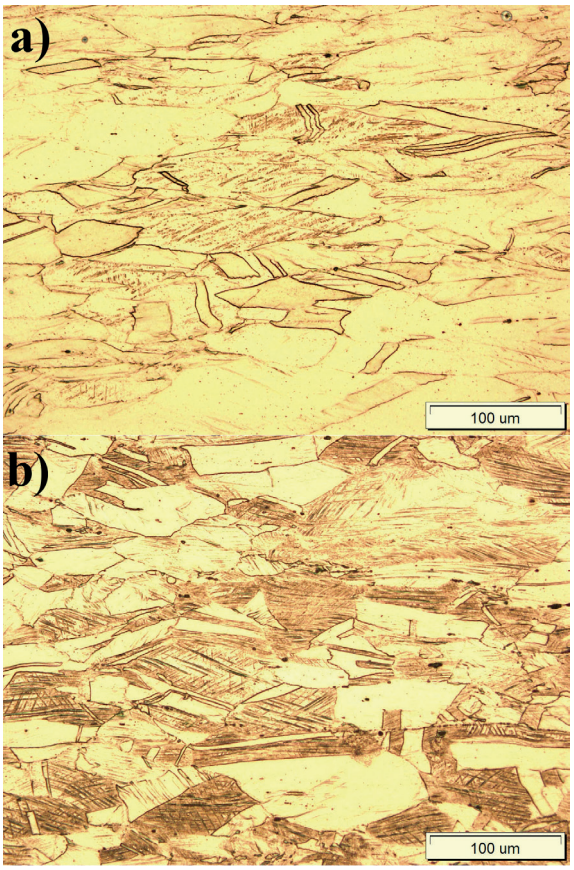

Fig. 1. Austenitic microstructure of the thermomechanically treated (a) and cold worked (b) X6MnSiAlNbTi26-3-3 steel

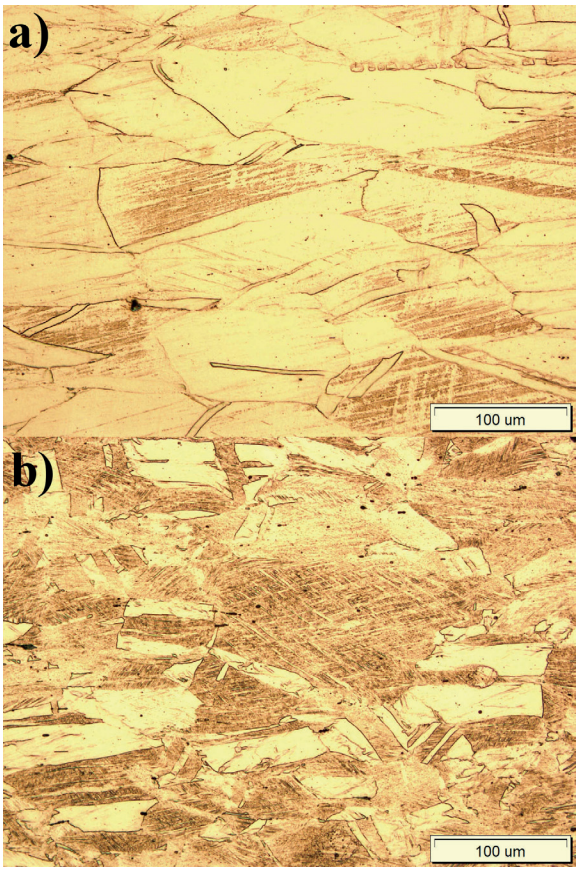

Fig. 2. Austenitic microstructure of the thermomechanically treated (a) and cold worked (b) X4MnSiAlNbTi27-4-2 steel

Results of our previous investigations [14] showed that both steels independently on their state (thermomechanically treated or cold worked) are characterized by the microstructure consisting of 100% austenite.

3.2. Electrochemical tests

In order to study the effect of non-metallic inclusions on the corrosion resistance of high-Mn steels, the potentiodynamic polarization tests in 3.5% NaCl solution were performed. Selected results of measurements obtained for X6MnSiAlNbTi26-3-3 and X4MnSiAlNbTi27-4-2 steel specimens for their different states are shown in Fig. 3a-b. Corrosion resistance of the both thermomechanically processed specimens was compared. Additionally, the influence of cold deformation on the corrosion parameters was analyzed. Average values of corrosion current density I_{corr} and corrosion potential E_{corr} of investigated steels, which were determined by the Tafel slope extrapolation are shown in Fig. 4a-b.

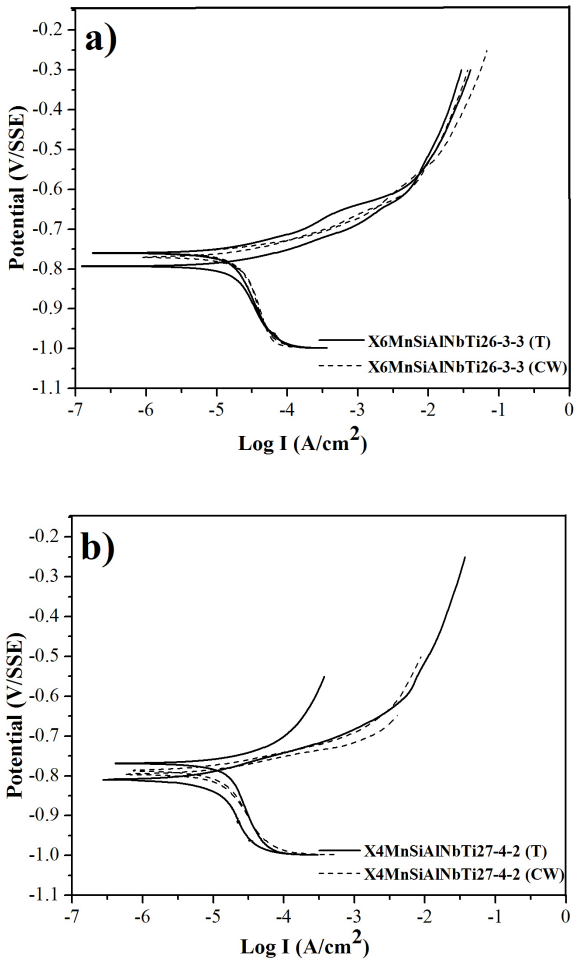

Fig. 3. Potentiodynamic polarization curves of the X6MnSiAlNbTi26-3-3 (a), and X4MnSiAlNbTi27-4-2 (b) thermomechanically treated and cold deformed steels obtained in 3.5% NaCl solution

Results of potentiodynamic polarization tests conducted in 3.5% NaCl solution, showed that the thermomechanically treated X4MnSiAlNbTi27-4-2 steel specimens are

characterized by higher corrosion current density (0.09 mA/cm^2) in comparison to the thermomechanically treated X6MnSiAlNbTi26-3-3 steel (0.009 mA/cm^2). Corrosion current density of high-Mn steels is significantly higher in acidic solutions [14]. Similar results were collected for cold deformed steel specimens. X4MnSiAlNbTi27-4-2 steel showed higher corrosion current density when compared to the X6MnSiAlNbTi26-3-3 steel. Cold deformation increased the corrosion current density to approximately 0.121 mA/cm^2 for the X4MnSiAlNbTi27-4-2 steel and to 0.026 mA/cm^2 for the X6MnSiAlNbTi26-3-3 steel. In general, cold-worked specimens show less resistance to corrosion initiation. It confirms our earlier results of a weight loss method [15]. Ghayad et al. [12] also reported that cold deformation decreases corrosion resistance of high-Mn steels. However, average value of corrosion current density registered for the cold deformed X6MnSiAlNbTi26-3-3 steel was lower than those ones measured for the thermomechanically processed steel containing below 2% Al.

Values of corrosion potential E_{corr} were quite similar for both steels independently on their state (Fig. 4b). For the X4MnSiAlNbTi27-4-2 steel, the average values of corrosion potential were: -788 mV and -780 mV for thermomechanically treated and cold worked specimens, respectively. For the X6MnSiAlNbTi26-3-3 steel: -785 mV (thermomechanically treated specimens) and -783 mV (cold deformed specimens).

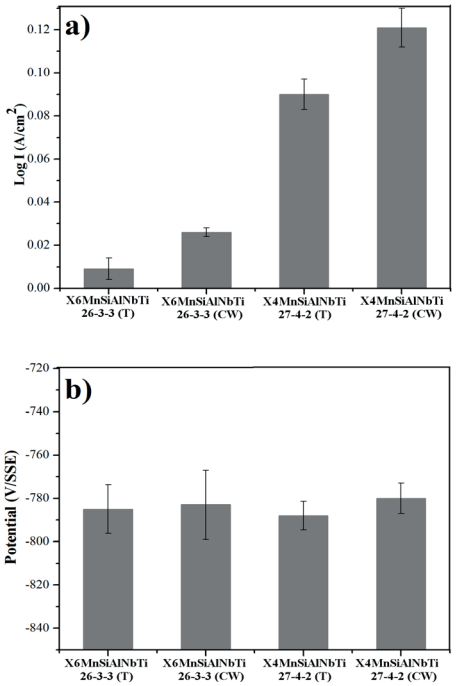

Fig. 4. Average values of electrochemical polarization data: (a) corrosion current density, (b) corrosion potential of thermomechanically processed and cold worked steels registered in 3.5% NaCl solution

TABLE 2

Results of EDS analysis of the individual pit (interior), formed in thermomechanically treated X4MnSiAlNbTi27-4-2 and cold deformed X6MnSiAlNbTi26-3-3 steels after corrosion tests

	Chemical composition of inclusion		Type of inclusion	Figure
	at. (%)	wt. (%)		
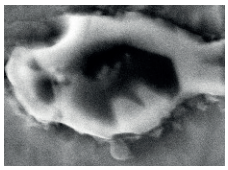	N (27.04), Al (37.98), S (11.89) Mn (14.06), Fe (09.04)	N (12.37), Al (33.47), S (12.45), Mn (25.22), Fe (16.49)	complex MnS+AlN	6c
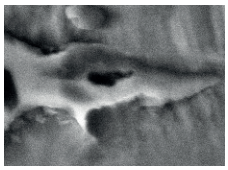	O (45.85), Al (06.00), Si (10.38), Mn (10.06), Fe (27.70)	O (22.32), Al (04.93), Si (08.87), Mn (16.81), Fe (47.07)	oxides containing Mn, Al and Si	6d
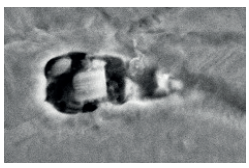	N (21.80), Al (39.78), S (08.01), Mn (13.70), Fe (16.71)	N (09.19), Al (32.31), S (07.73), Mn (22.66), Fe (28.10)	complex MnS+AlN	8c
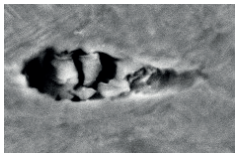	N (10.33), O (06.80), Al (36.39), Si (02.24), S (10.26), Mn (15.53), Fe (18.45)	N (04.12), O (03.10), Al (27.97), Si (01.79), S (09.37), Mn (24.30), Fe (29.35)	complex oxysulphides containing Mn, S, Al, N, Si	8d

3.3. Pitting behaviour

The morphology of corrosion pits after the electrochemical tests were studied by SEM and using EDS techniques. SEM images of corrosion damage occurred in both steels after corrosion tests in 3.5% NaCl are shown in Figs. 5 and 6 for the thermomechanically treated X4MnSiAlNbTi27-4-2 steel and in Figs. 7 and 8 for the cold deformed X6MnSiAlNbTi26-3-3 steel. Results of EDS analysis of the individual pit (interior), formed in thermomechanically treated X4MnSiAlNbTi27-4-2 and cold deformed X6MnSiAlNbTi26-3-3 steels after corrosion tests are summarized in Table 2.

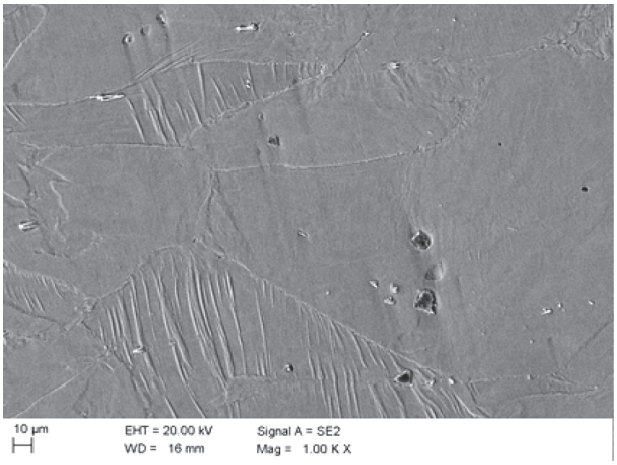

Fig. 5. SEM micrograph of the thermomechanically treated X4MnSiAlNbTi27-4-2 steel surface after corrosion test in 3.5% NaCl

Corrosion damage formed in the thermomechanically treated X4MnSiAlNbTi27-4-2 steel is characterized by various shapes and an irregular distribution at the metallic matrix (Fig. 5). Corrosion pits are generated both in grain interiors and grain boundaries (Fig. 6a). The pit nucleation sites were analysed by SEM equipped with EDS. The chemical composition of the particle inside the pit in Fig. 6b showed the high content of manganese, sulfur, aluminium and nitrogen (Fig. 6c). It indicates that the privileged places for the pit initiation are complex inclusions composed of MnS and AlN. The chemical analysis of corrosion damage shown in Fig. 6b revealed the presence of oxides containing Mn, Al and Si (Fig. 6d). Park et al. [6] also observed the presence of complex inclusions, such as MnS + AlN in high-Mn steels. Moreover, complex MnS + Al_2O_3 particles were also identified.

SEM images of the cold deformed X6MnSiAlNbTi26-3-3 steel after corrosion tests in 3.5% NaCl show good agreement with the results of potentiodynamic tests. Higher corrosion current density obtained for cold deformed specimens is reflected by increasing amount of corrosion damage, which formed on the non-metallic inclusions (Fig. 7). The corrosion pits are preferentially initiated along grain boundaries, inside the austenite grains and along the deformation bands (Fig. 8a). EDS analysis of the individual pit in Fig. 8b revealed the high content of Mn, S, Al and N (Fig. 8c). It indicates that in the X6MnSiAlNbTi26-3-3 cold deformed steel, the corrosion pits are formed at inclusions composed of MnS and AlN too.

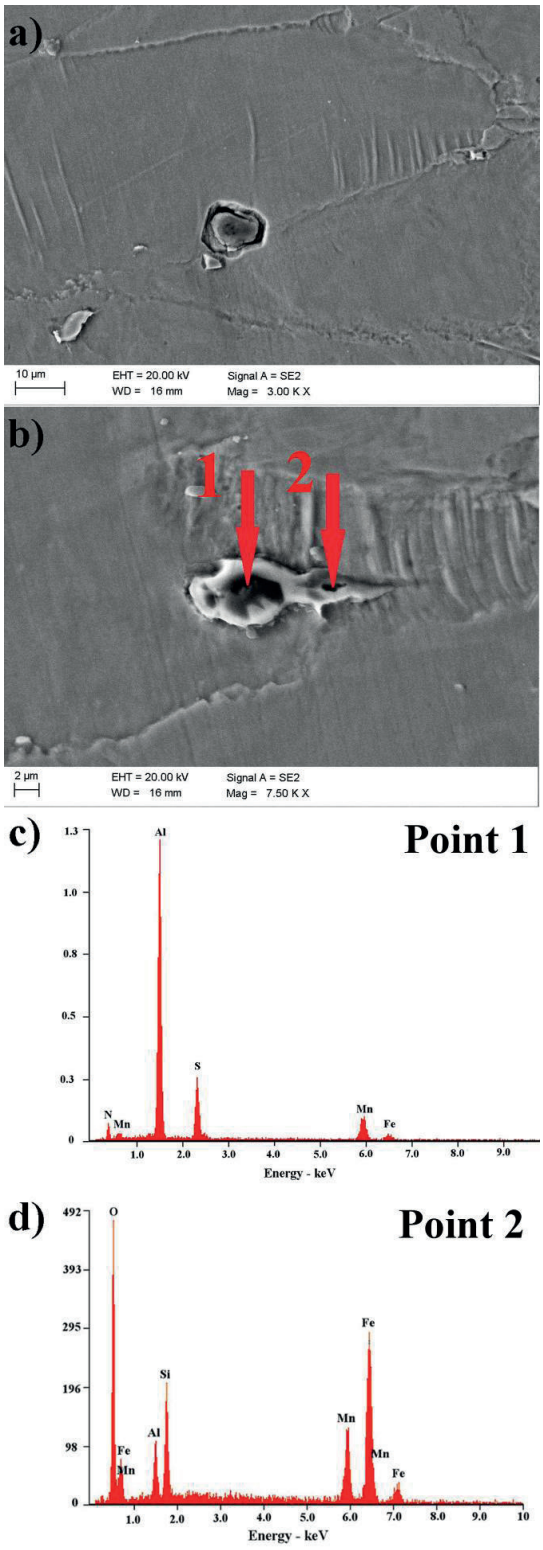

Fig. 6. SEM micrographs of the thermomechanically treated X4MnSiAlNbTi27-4-2 steel surface (a), the individual pit interior (b) and EDS analyses from the point 1 (c) and point 2 (d)

The chemical composition of the particle inside the corrosion pit in Fig. 8b showed the presence of elements such as: Al, N, Mn, S, O and Si (Fig. 8d). The results of SEM observation and EDS analysis confirmed our earlier results [16] and supports the data reported by other authors [6-10]. It means that corrosion pits are initiated mainly at non-metallic inclusions such as MnS, AlN and at complex oxysulphides.

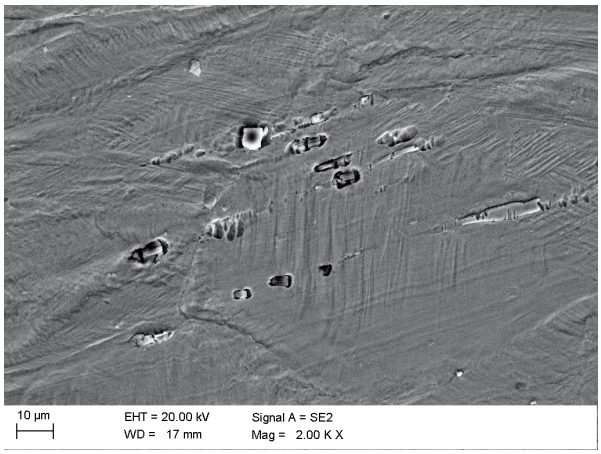

Fig. 7. SEM micrograph of the cold deformed X6MnSiAlNbTi26-3-3 steel surface after corrosion test in 3.5% NaCl

4. Discussion

4.1. Effect of non-metallic inclusions on the corrosion resistance and pitting behaviour

Results of corrosion tests of X4MnSiAlNbTi27-4-2 and X6MnSiAlNbTi26-3-3 steels show relations between their corrosion resistance and the presence of non-metallic inclusions. It has been reported [16-18] that elements such as manganese and sulfur have a negative influence on the corrosion resistance of high-Mn steels. Manganese combines with sulfur creating MnS inclusions, which are vulnerable for pitting corrosion attack [6-10, 19]. Schmuki et al. [7] found that for the stainless steels pitting corrosion during immersion in a 10% $FeCl_3$ solution always started at MnS inclusions. The amount of MnS inclusions depends primarily on the sulfur content. Increasing the sulfur content causes the increase of MnS quantity. An explanation for the lower corrosion resistance of the X4MnSiAlNbTi27-4-2 steel is the higher S content of 0.017 wt.% when compared to the X6MnSiAlNbTi26-3-3 steel (0.013 wt.%). It seems that sulfur deteriorates the corrosion resistance, thus higher corrosion current values were detected for the X4MnSiAlNbTi27-4-2 steel. Park and Kwon [17] found that a size of MnS inclusions increased with the increase Mn concentration in Fe–18Cr–6Mn and Fe–18Cr–12Mn steels. Therefore, corrosion processes occurring in the X4MnSiAlNbTi27-4-2 steel could be also to a lesser extend accelerated by the higher Mn content.

The investigated steels contain silicon and aluminium additions, which are characterized by high chemical affinity to oxygen (aluminium also to nitrogen). Park et al. [6] reported that DP steel with single MnS inclusions was characterized by worse resistance to pitting corrosion than TRIP steel containing single AlN inclusions. EDS analysis of corrosion pits formed in the X4MnSiAlNbTi27-4-2 (Fig. 6c-d) and X6MnSiAlNbTi26-3-3 (Fig. 8c-d) steels revealed presence of MnS and AlN inclusions in both steels. In the steel containing a higher amount of Al, Al_2O_3 particles were also detected. It is reported [6] that Al_2O_3 inclusions are characterized by higher corrosion resistance than MnS and AlN particles. Hence, better corrosion resistance of the X6MnSiAlNbTi26-3-3 steel could be related to higher Al_2O_3- and lower quantity of MnS inclusions. Corrosion damage formed in both high-Mn steels are characterized by various size and shapes (Fig. 5 and Fig. 7). Abbasi Aghuy et al. [20] observed similar results in stainless steels after corrosion test in 3.5% NaCl. Williams et al. [8] reported that in stainless steels, the control of the composition, density and size of the inclusions has a critical effect on the probability of initiation of pitting corrosion.

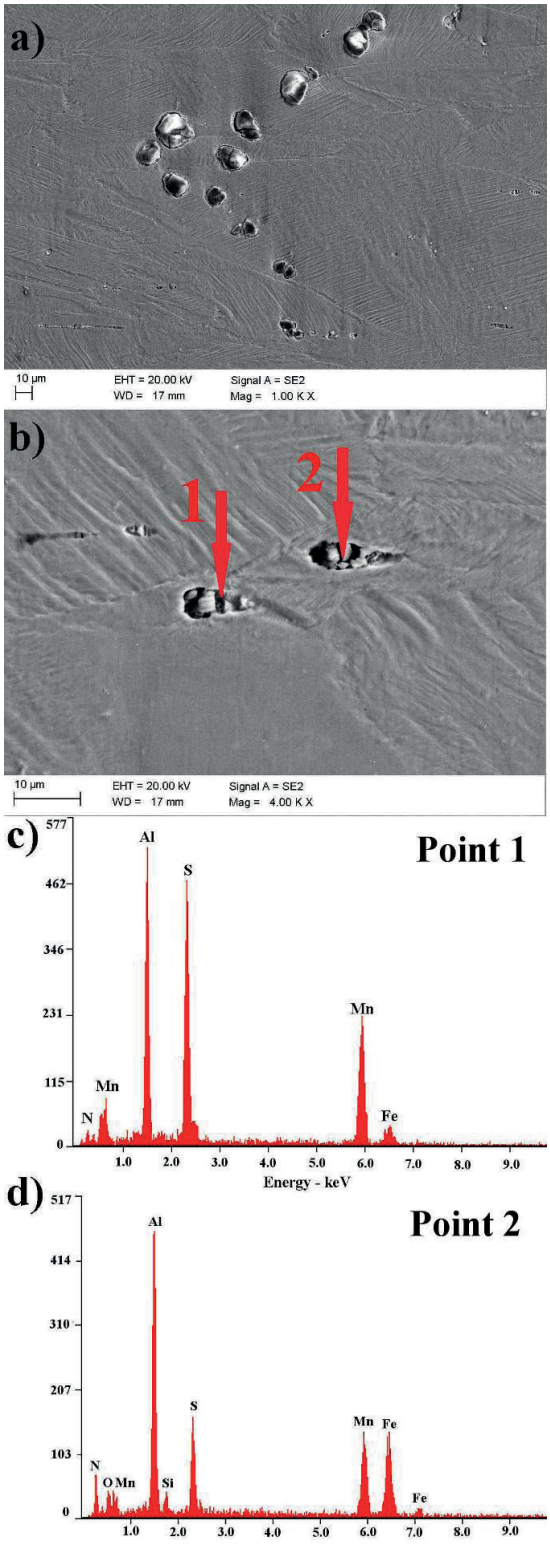

Fig. 8. SEM micrograph of the cold deformed X6MnSiAlNbTi26-3-3 steel surface (a), the individual pit interiors (b) and EDS analyses from the point 1 (c) and point 2 (d)

Better corrosion resistance of the X6MnSiAlNbTi26-3-3 steel is attributed to higher Al and lower Si contents in comparison to the X4MnSiAlNbTi27-4-2 steel (Table 1). It confirms our earlier results of potentiodynamic polarization tests [14, 21]. It is well known, that aluminium improves corrosion resistance of steel due to its tendency to formation of the protective Al_2O_3 passive layer on the steel surface in solutions of pH about 7 (Pourbaix diagrams), which increased slightly the corrosion resistance of the investigated steel [22]. It is also reported [23] that silicon addition decreases corrosion resistance of steel.

4.2. Effect of cold deformation on the corrosion resistance

Electrochemical measurements presented in this work show that cold deformation affects strongly corrosion resistance of investigated alloys. In comparison to both X4MnSiAlNbTi27-4-2 and X6MnSiAlNbTi26-3-3 thermomechanically processed steel specimens, the cold deformed specimens were characterized by higher corrosion current density (Fig. 4a). It confirms our earlier results of potentiodynamic tests [14] and supports the data reported by other authors [12-15, 24-26]. The values of corrosion potential are similar for thermomechanically treated and cold deformed specimens (Fig. 4b). SEM micrographs showed that amount of corrosion pits formed in cold deformed steel (Fig. 8a) was higher than observed in thermomechanically processed steel (Fig. 6a).

It is worth to note that corrosion damage formed in both investigated steels are characterized by various shapes and an irregular distribution at the metallic matrix (Fig. 5 and Fig. 7). Corrosion pits are generated both in grain interiors and at grain boundaries. Additionally, corrosion damage occurred along the deformation bands (Fig. 8a). Corrosion properties are attributed to the defects density, i.e., high dislocation density at the grain boundaries increased by cold deformation. It leads finally to reduction of corrosion resistance. These regions were particularly vulnerable for pit nucleation. Larger amount of deformation twins present in the microstructure of the cold deformed steels also contributes to lowering its corrosion resistance, due to the difference in potentials between the matrix and twin, which create local corrosion cells.

Formation of second phase within the austenitic matrix, as a result of heat treatment or plastic deformation can increase the corrosion current density [13-15]. A different phase forms a galvanic couple, which accelerates the corrosion rate. In our previous study [14], X-ray diffraction patterns obtained both for thermomechanically processed and cold worked specimens confirmed a homogeneous austenitic microstructure. Consequently, the lower corrosion resistance of cold deformed steel specimens is not related to a multiphase structure but to chemical composition and plastic deformation.

5. Conclusions

Corrosion resistance of high-Mn steels is related to the type and amount of non-metallic inclusions. EDS analysis of corrosion damage formed in the X6MnSiAlNbTi26-3-3 and X4MnSiAlNbTi27-4-2 steels after corrosion tests in 3.5% NaCl confirmed that corrosion pits nucleated preferentially on the MnS, AlN inclusions and complex oxysulphides containing Mn, Al and Si. Higher contents of manganese, sulfur and silicon combined with a lower content of aluminium is reflected in the worse corrosion resistance of the X4MnSiAlNbTi27-4-2 steel.

The chemical composition of the steels does not affect the privileged areas of pits nucleation. Corrosion damage formed in both investigated steels is characterized by an irregular distribution at the metallic matrix, independently on a steel state. Corrosion pits are generated both in grain interiors, grain boundaries and along the deformation bands. Cold deformation deteriorates corrosion resistance. A number of corrosion pits in cold deformed steels is higher than in thermomechanically treated steels. It is related to greater dislocation density and formed deformation twins. However, the cold deformed steel containing the higher Al (~3%) content and smaller Si (~3%) content shows better corrosion resistance in comparison to the thermomechanically processed X4MnSiAlNbTi27-4-2 steel, indicating the fundamental significance of chemistry related to Al and Si alloying.

Acknowledgment

This publication was financed by the Ministry of Science and Higher Education of Poland as the statutory financial grant of the Faculty of Mechanical Engineering SUT.

REFERENCES

[1] G. Frommeyer, U. Brüx, P. Neumann, ISIJ Int. **43**, 438-446 (2003).
[2] L.A. Dobrzański, A. Grajcar, W. Borek, Mater. Sci. Forum **638-642**, 3224-3229 (2010).
[3] A. Grajcar, U. Galisz, L. Bulkowski, Arch. Mater. Sci. Eng. **50**, 21-30 (2011).
[4] P. Kaushik, H. Yin, Iron & Steel Technol. **9**, 165-185 (2012).
[5] A. Grajcar, R. Kuziak, Adv. Mater. Res. **314-316**, 119-122 (2011).
[6] I.J. Park, S.M. Lee, M. Kang, S. Lee, Y.K. Lee, J. Alloy. Compd. **619**, 205-210 (2015).
[7] P. Schmuki, H. Hildebrand, A. Friedrich, S. Virtanen, Corros. Sci. **47**, 1239-1250 (2005).
[8] D.E. Williams, M.R. Kilburn, J. Cliff, G.I.N. Waterhouse, Corros. Sci. **52**, 3702-3716 (2010).
[9] H. Krawiec, V. Vignal, O. Heintz, R. Oltra, Electrochim. Acta **51**, 3235-3243 (2006).
[10] T.V. Shibaeva, V.K. Laurinavichyute, G.A. Tsirlina, A.M. Arsenkin, K.V. Grigorovich, Corros. Sci. **80**, 299-308 (2014).
[11] A. Grajcar, A. Płachcińska, S. Topolska, M. Kciuk, Mater. Tehnol. **49**, (6), 889-894 (2015).
[12] I.M. Ghayad, A.S. Hamada, N.N. Girgis, W.A. Ghanem, Steel Grips **4**, 133-137 (2006).
[13] Y.S. Chun, J.S. Kim, K.T. Park, Y.K. Lee, C.S. Lee, Mater. Sci. Eng. A **533**, 87-95 (2012).
[14] A. Grajcar, M. Kciuk, S. Topolska, A. Płachcińska, J. Mater. Eng. Perform. **25**, doi: 10.1007/s11665-016-2085-5 (2016).
[15] A. Grajcar, W. Krukiewicz, S. Kołodziej, J. Achiev. Mater. Manuf. Eng. **43**, 228-235 (2010).

[16] A. Grajcar, A. Płachcińska, Mater. Tehnol. **50**, (5), (2016) (in press).
[17] K.J. Park, H.S. Kwon, Electrochim. Acta **55**, 3421-3427 (2010).
[18] A. Pardo, M.C. Merino, A.E. Coy, F. Viejo, R. Arrabal, E. Matykina, Corros. Sci. **50**, 1796-1806 (2008).
[19] C. Donik, I. Paulin, M. Jenko, Mater. Tehnol. **44**, 67-72 (2010).
[20] A. Abbasi Aghuy, M. Zakeri, M.H. Moayed, M. Mazinani, Corros. Sci. **94**, 368-376 (2015).
[21] A. Grajcar, S. Kołodziej, W. Krukiewicz, Arch. Mater. Sci. Eng. **41**, 77-84 (2010).
[22] N. Takeno, National Institute of Advanced Science and Technology, Tokyo (2005).
[23] S. Suzuki, E. Matsubara, T. Komatsu, Y. Okamoto, K. Kanie, A. Muramatsu, H. Konishi, J. Mizuki, Y. Waseda, Corros. Sci. **49**, 1081-1096 (2007).
[24] A. Kurc, M. Kciuk, M. Basiaga, J. Achiev. Mater. Manuf. Eng. **38**, 154-162 (2010).
[25] Y. Fu, X. Wu, E.H. Han, W. Ke, K. Yang, Z. Jiang, Electrochim. Acta **54**, 1618-1629 (2009).
[26] M. Jabłońska, R. Michalik, Solid State Phenom. **227**, 109-112 (2015).